Analytic prediction of the exact thermodynamics of a first-order structural phase transition: A practical second-order self-consistent phonon theory

J. R. Morris*
Laboratory of Atomic and Solid State Physics, Cornell University, Ithaca, New York 14853-2501

R. J. Gooding
Department of Physics, Queen's University, Kingston, Ontario, Canada K7L 3N6
(Received 11 March 1992)

We examine an extension of self-consistent phonon theory (SCPT) that allows for the explicit evaluation of second-order corrections to the free energy for both the high- and low-temperature phases for a system undergoing a first-order structural phase transition. The motivation for the inclusion of these terms stemmed from the many-body theory developed to treat the lattice vibrations in anharmonic crystals. This approach does not modify predictions for the phonon frequencies that would be observed by inelastic neutron scattering; however, we show that these higher-order contributions to the free energy are *essential* if the bulk limit of the equilibrium thermodynamic quantities are to be forecast accurately. Finite-size scaling is used to extrapolate the bulk limit, and we present arguments showing that precursor fluctuations are not allowed in bulk systems that are truly ergodic. Thus, in part the effectiveness of our second-order SCPT may be understood by noting the absence of large-amplitude fluctuations. In addition, dynamical structure factors, calculated using molecular-dynamic simulations, for systems of a strip geometry, show sharp phonon peaks at the SCPT frequencies, with lifetimes much longer than phonon periods—these lifetimes grow as one approaches the bulk limit.

I. INTRODUCTION

The calculation of the total free energy (electronic plus ionic) of crystals from microscopic Hamiltonians is an important challenge. In recent years advances in first-principle electronic structure calculations have provided us with sound quantitative knowledge of the ground-state energy of the electronic degrees of freedom, and from the electronic density-of-states information on the electronic entropy follows immediately. In addition to these quantities, first-principles calculations have also allowed for the accurate calculation of electron-phonon couplings. Then, utilizing the Born-Oppenheimer approximation, the restoring forces (harmonic plus anharmonic) for the ionic motion follow, and thus we are now in a position where quantitative estimates of the thermodynamic properties (based on both the electronic and ionic energetics) of crystals can be made from first principles. One example of executing this approach, in part utilizing the so-called frozen phonon method (a technique well suited for ionic displacements involving high-symmetry phonons) may be found in the work done by Ye, Chen, Harmon, and coworkers.[1-4]

For certain systems, in which the lattice dynamics are essentially harmonic, the calculation of the ionic free energy is then straightforward. The phonon frequencies are calculated by truncating the ionic Hamiltonian at terms second-order in the displacements, and from this the harmonic lattice vibrational free energy may be determined directly. Inclusion of the anharmonic terms in an expansion of the ionic potential is most easily treated by using a *self-consistent* technique, in which the phonon frequencies become temperature dependent.[5] This is a first-order variational technique known as the self-consistent phonon theory (hereafter referred to as SCPT), the product of which is a set of weakly temperature-dependent phonon frequencies, and the lattice free energy. Then, direct comparisons may be made to the phonon dispersion curves measured in inelastic neutron-scattering studies.

Systems undergoing first-order structural transitions, however, are highly anharmonic. These systems undergo transitions that are characterized by the discontinuous "freezing in" of a lattice displacement, viz. a phonon mode and/or a lattice strain. Due to the inherent strong nonlinearities in these systems, it is not clear that a simple perturbative approach such as SCPT will work. Alternatively, some justification of the use of SCPT in such strongly anharmonic systems is necessary. For example, when applied to some other transitions, the approach simply doesn't work: for the widely studied ϕ^4 model of second-order structural transitions, SCPT incorrectly predicts a first-order transition.[6,7]

We begin our discussion of the work we have conducted concerning a second-order SCPT by firstly noting that the usual implementation of (first-order) SCPT has the drawback that cubic and higher-order odd-power anharmonicities in the ionic potential energy do not contribute to the free energy. Some second-order variational techniques[8,9] have been suggested to remove this drawback. They are, however, quite difficult to implement, to the point of being impractical. Further, the use of the second-order free energy as a variational expression[8,9] is unjustified.

We wish to draw attention to motivation for going

beyond the usual SCPT and insisting that some account of the cubic and other odd-power anharmonicities must be taken when evaluating the free energy. It is known, from the many-body theory developed to deal with anharmonic lattice vibrations,[10] that even though the terms that are fourth-order in displacements are higher order than the third-order terms, because of limitations in reciprocal space,[11] the fourth-order terms are equally as important. To be specific, by contributing to the real part of the self-energy of the phonon Green's function, the fourth-order terms cause a renormalization of the phonon frequencies. This is the lowest-order perturbative correction to the frequencies. In contrast, the third-order terms do not affect the phonon frequencies to first order; however, they do contribute to the second-order corrections, and more importantly they provide the dominant perturbative contribution to the reduction of the phonon lifetimes.[10] Thus, the third-order terms may have a significant effect on the thermodynamic quantities (see the discussion in Ref. 11). No account, that we are aware of, has been previously developed that allows for the incorporation of these second-order effects, including the phonon lifetimes, into SCPT in such a way that the formalism may be tested by comparison either with exact results or with experimental systems. This paper aims to remedy this deficiency. The purpose of this paper is to propose a simple extension of SCPT and to demonstrate the practicality of the scheme. Also, we will show that our approach reproduces the free energy for first-order structural transitions with remarkable precision, the accuracy being greatly enhanced by inclusion of the second-order contributions.

Motivation for our approach may also be found in experimental studies of systems exhibiting first-order diffusionless structural phase transitions. Most diffusionless structural transitions are first-order, exhibiting little overt anharmonicity, viz., phonon softening.[12] Further, for a large class of these transitions, the latent heat at the transition is mainly due to the change in the vibrational entropy,[13] indicating the importance of understanding the lattice contribution to the free energy. Thus, some impetus for this work has been the complimentary experimental work demonstrating that the dynamics of these systems are nearly harmonic, even at temperatures very close to the transition.[13] For example, inelastic neutron-scattering studies of pure, single-crystal Group IV metals have shown that the frequencies of phonons associated with the bcc$\rightarrow$hcp transition decrease slightly with temperature to a finite frequency at the transition. There are no indications of "heterophase" fluctuations—strongly nonlinear modes connecting the high- and low-temperature phases. These results strongly suggest an approach such as SCPT, which is best for systems with small amplitude vibrations.

We have been studying a simple model for such vibrational-entropy driven transitions.[14–16] The exact thermodynamics describing this system demonstrate that heterophase fluctuations may occur only in a small, finite-size affected temperature regime near the transition.[16] This regime vanishes rapidly as the bulk limit is approached, and is strongly sensitive to the change in the vibrational entropy. Outside of this regime, the dynamics are essentially harmonic, due to the absence of large amplitude fluctuations. SCPT has provided a good approximation to one-dimensional results for the exact free energy of this model, and molecular-dynamics simulations have shown that the dynamical structure factor has sharp phonon peaks at frequencies very close to those predicted by SCPT.[15] Here we extend our consideration of this model to examine the comparison of the analytic second-order SCPT prediction for the thermodynamics to the now-known exact thermodynamics (in the bulk limit) for this model,[16] as well as the familiar first-order SCPT.

Our paper is organized as follows. In Sec. II, we present the formalism for our extension of SCPT; a model of a vibrational-entropy driven first-order phase transition[14] will be discussed as an example to which this technique may be applied. In Sec. III finite-size systems are examined via the strip-transfer matrix formalism, and a finite-size scaling ansatz for first-order, symmetry-breaking, temperature-driven phase transitions is presented. This allows for the extrapolation of exact thermodynamic quantities, which we then compare to the results obtained from our second-order SCPT. In fact, these results show that the approximate second-order SCPT free energy reproduces the exact results to within 0.1%, with the agreement improving as the system size is increased. This allows us to perform a very precise determination of the bulk transition temperature. Molecular-dynamic simulations are presented in Sec. IV, and these results allow us to understand the success of the second-order SCPT via the rapid approach of the dynamic structure factor to the quasiharmonic limit as the system size is increased. Our results will be summarized and outstanding questions discussed in Sec. V.

II. FORMALISM AND MODEL HAMILTONIAN

We begin our considerations of the second-order free energy contributions by first recalling that the first-order perturbative result for the free energy provides an upper bound for the true free energy. Although we derive this classically, the result is generally true.[17] To calculate the free energy for N configurational degrees of freedom from the microscopic potential $V(\{u_i\})$, $i=1,\ldots,N$, it is necessary to calculate the partition function. Classically, the partition function may be expressed as $Z=Z_c Z_p$, where Z_c is the configurational partition function, and Z_p is the momentum part of the partition function

$$Z_p=\left[\frac{2\pi mT}{\hbar^2}\right]^{N/2} . \tag{1}$$

The configurational partition function is given by

$$Z_c=\int du_1\cdots du_N \exp[-\beta V(\{u_i\})] . \tag{2}$$

We are free to express the potential in terms of a trial function plus a perturbation:

$$V(\{u_i\})=V_t(\{u_i\})+\lambda V_{\text{pert}}(\{u_i\}) . \tag{3}$$

The configurational contribution to the free energy is

$$F \equiv -T \ln Z_c \ , \tag{4}$$

which may be expressed in a perturbation sequence in λ:

$$F = F_0 - \sum_{n=1}^{\infty} \frac{(-\lambda)^n \langle V_{\text{pert}}^n \rangle_{t,c}}{n! T^{n-1}} \ . \tag{5}$$

The notation $\langle \cdots \rangle_{t,c}$ indicates a cumulant expansion. Here, the unperturbed free energy is given by

$$\exp[-\beta F_0] \equiv Z_t = \int du_1 \cdots du_N \exp[-\beta V_t(\{u_i\})] \tag{6}$$

and the averages are with respect to the trial potential:

$$\langle (\cdots) \rangle_t \equiv \frac{1}{Z_t} \int du_1 \cdots du_N (\cdots) \exp[-\beta V_t(\{u_i\})] \ . \tag{7}$$

To second order in λ, the free energy is then given by

$$F \approx F_0 + \lambda \langle V_{\text{pert}} \rangle_t - \frac{\lambda^2}{2T} (\langle V_{\text{pert}}^2 \rangle_t - \langle V_{\text{pert}} \rangle_t^2) \ . \tag{8}$$

Using this result, it is straightforward to show that the curvature $\partial^2 F / \partial \lambda^2$ is always negative;[17] thus the first-order result provides an upper bound to the true free energy

$$F \leq F_0 + \lambda \langle V_{\text{pert}} \rangle_t \ . \tag{9}$$

SCPT is the direct application of Eq. (9); to be specific, V_t chosen to be second order (viz., harmonic) in the displacements $\{u_i\}$. Then, the right-hand side of Eq. (9) is minimized with respect to the ionic coupling constants; this yields a *self-consistent* set of equations for these constants, and leads to the best possible first-order estimate of the free energy. Equivalently, the frequency of each phonon mode may be determined. From these temperature-dependent phonon frequencies the variational free energy follows immediately.

While the above treatment is straightforward, there are reasons to go beyond this approximation. Note that terms in V_{pert} involving odd powers of the displacements do not contribute to the right-hand side of Eq. (9) due to the symmetry of the harmonic states used in the thermal average, viz., $\{u_i\} \rightarrow \{-u_i\}$. For systems undergoing first-order structural transitions, dominant corrections to the first-order result can be accounted for by using the second-order expression, Eq. (8), which directly incorporates these odd-power terms to produce a considerably improved result. (Contributions to the free energy from domain walls and heterophase fluctuations are nonperturbative corrections, but these contributions are vanishingly small as the bulk limit is approached, and are negligible when compared to higher-order perturbative corrections.[16] In contrast to this, the second-order correction is significant, even in the bulk limit, as we shall demonstrate in Sec. III.)

To make the above ideas more concrete, and to demonstrate the modifications that we have incorporated, we apply them to the following model potential for particles on a square lattice:

$$V(u_i) = \sum_{\mathbf{i}} \left[V_{os}(u_{\mathbf{i}}) + \frac{k_x}{2}(u_{\mathbf{i}} - u_{\mathbf{i}+\hat{\mathbf{x}}})^2 + \frac{k_y}{2}(u_{\mathbf{i}} - u_{\mathbf{i}+\hat{\mathbf{y}}})^2 + \frac{\alpha_x}{4}(u_{\mathbf{i}}^2 + u_{\mathbf{i}+\hat{\mathbf{x}}}^2)(u_{\mathbf{i}} - u_{\mathbf{i}+\hat{\mathbf{x}}})^2 + \frac{\alpha_y}{4}(u_{\mathbf{i}}^2 + u_{\mathbf{i}+\hat{\mathbf{y}}}^2)(u_{\mathbf{i}} - u_{\mathbf{i}+\hat{\mathbf{y}}})^2 \right] \ . \tag{10}$$

The lattice vectors are $\hat{\mathbf{x}}$ and $\hat{\mathbf{y}}$, and $u_{\mathbf{i}}$ is the *scalar* displacement of particle $\mathbf{i}$. (Note that while we consider a system defined on a square lattice, the above Hamiltonian has, in general, rectangular symmetry, due to the possibility of anisotropic coupling constants. In our own analysis we preserve the square symmetry by requiring $k_x = k_y$ and $\alpha_x = \alpha_y$.) The on-site potential is

$$V_{os}(u) = \frac{A}{2}u^2 - \frac{B}{4}u^4 + \frac{C}{6}u^6 \ . \tag{11}$$

This model describes a simple system undergoing a first-order symmetry-breaking structural phase transition; the order parameter is the average displacement $\langle u \rangle$. The one-site potential is shown schematically in Fig. 1. At high temperatures, the system will be localized in the center well; hence the mean displacement will be zero. At low temperatures the system is localized in one of the side wells, so the displacement is nonzero. It is important to realize that the system will have a true phase transition (i.e., a nonzero value of $\langle u \rangle$) only in two (or greater) dimensions, and only in the thermodynamic limit.[16] For

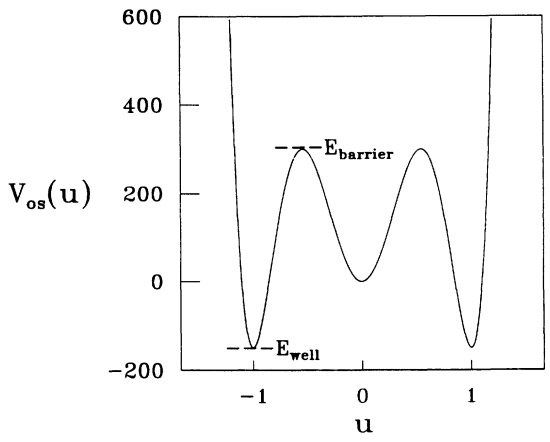

FIG. 1. The nonlinear on-site potential energy $V_{os}(u)$ that localizes each particle to a lattice site. By setting the energy scale so that $E_{\text{barrier}} = 300$ and the length scale so that the minima are at $u = \pm 1$, the remaining parameter specifying the potential is chosen to be the ratio $E_{\text{barrier}} / E_{\text{well}}$.

finite systems, the average displacement is identically zero at all temperatures due to the $u \rightarrow -u$ symmetry of the Hamiltonian.

The on-site potential of Eq. (11) is specified by three parameters. By choosing a length scale and an energy scale, only one parameter remains. We have chosen the length scale so that the absolute minimum in the potential occur at $u=\pm 1$, and the energy scale such that the energy barriers have the energy $E_{\text{barrier}}=300$ (see Fig. 1). The remaining parameter we are free to choose, and represents the ratio of the barrier height energy to the well depth energy $E_{\text{barrier}}/E_{\text{well}}$.

The anharmonic couplings of strength α_x,α_y have been introduced in order to mimic the change in dispersion that occurs at the transition. These couplings directly alter the change in entropy at the transition.[14] In the high-temperature phase, when $\langle u^2\rangle \ll 1$, these couplings have little effect: the interactions are nearly harmonic, with strengths k_x,k_y. In the low-temperature phase, when $\langle u^2\rangle \approx 1$, the couplings are approximately harmonic, with strengths $k_x+\alpha_x,k_y+\alpha_y$. Thus, the dispersion of the phonons is altered in the low-temperature phase by the inclusion of the anharmonic intersite coupling.

To calculate the approximate free energy, we introduce the trial harmonic potential

$$V_t=\sum_i \left[\frac{1}{2}\Omega^2 y_i^2+\frac{\phi_x}{2}(y_i-y_{i+\hat{x}})^2+\frac{\phi_y}{2}(y_i-y_{i+\hat{y}})^2 \right] ,$$

$$y_i \equiv u_i-\bar{u} . \quad (12)$$

The average order parameter is indicated by $\bar{u}$. The variational parameters to be used in Eq. (9) are Ω^2, ϕ_x, ϕ_y, and $\bar{u}$. Note that in some implementations of SCPT, $\bar{u}$ is not treated as a variational parameter, but is fixed to be at the bottom of one of the wells of the on-site potential; we do not impose this restrictive choice. Instead, the free energy of the low-temperature phase is determined by setting $\bar{u}=1$; the high-temperature phase is determined by setting $\bar{u}=0$. By allowing $\bar{u}$ to be a variational parameter, odd-order terms that appear in the expansion of $V_{\text{os}}(u)$ about $u=\pm 1$ contribute to the first-order expression for the free energy. This produces considerably more accurate results.[7,17] However, odd-order terms in the expansion of the true potential about $\bar{u}$ still do not contribute to the variational estimate of F.

This first-order technique has been applied to the above Hamiltonian with excellent results.[15] To improve upon this, we have calculated the *second-order* expression for the free energy, Eq. (8). The parameters found from minimizing the first-order SCPT have been used in this evaluation. This allows for a direct contribution from the odd-order terms, via the $\langle V_{\text{pert}}^2\rangle_t$ term. Note that we have *not* minimized the second-order expression as has been suggested elsewhere;[8,9] for the uncoupled case ($k_x=k_y=\alpha_x=\alpha_y=0$) the second-order expression for the free energy may be made *arbitrarily negative* by the appropriate choice of parameters, clearly making this type of approach invalid. In general, the approximate free energy generated by Eq. (8) is not a rigorous upper bound to the true free energy, unlike results from Eq. (9). Further, in practice, such a minimization would be quite difficult for any realistic potential, due to the complexity of the expression for the second-order term. Note that although previous techniques[8,9] provided a method for calculating the phonon lifetimes, while we focus on the free energy, the phonon lifetimes and second-order corrections to the phonon frequencies may be calculated by using standard second-order expressions for the phonon self-energy,[10,11] and evaluating averages using the self-consistent values of the variational parameters. Again, this is a simpler approach than the alternate techniques.

The unperturbed (harmonic) part of the free energy may be expressed as

$$F_0=-\frac{T}{2}\sum_{\mathbf{q}} \ln\left[\frac{2\pi T}{\omega^2(\mathbf{q})}\right] . \quad (13)$$

The frequencies are given by

$$\omega^2(\mathbf{q})=\Omega^2+4\phi_x \sin^2\frac{q_x}{2}+4\phi_y \sin^2\frac{q_y}{2} . \quad (14)$$

The mathematics involved in calculating the first- and second-order corrections are simplified for classical systems using the pairing theorem,[18] which is the classical analogue of Wick's theorem. In real space, this may be phrased as

$$\langle y_{i_1}\cdots y_{i_{2n}}\rangle_t=\langle y_{i_1}y_{i_2}\rangle_t\cdots\langle y_{i_{2n-1}}y_{i_{2n}}\rangle_t+\text{all similar products of averages of pairs of variables.}$$

This leads to $(2n-1)(2n-3)\cdots$ terms representing the number of ways of grouping the variables into pairs. This is a direct result of using a harmonic trial potential: the modes are uncoupled, so the averages over differing modes may be computed independently.

Calculating the first-order result and minimizing with respect to Ω^2, ϕ_x, ϕ_y, and $\bar{u}$ gives the following self-consistent equations:

$$\Omega^2=A'-3B'\bar{u}^2+5C\bar{u}^4 , \quad (15a)$$

$$\phi_x=k_x+\alpha_x(\bar{u}^2+3\langle y^2\rangle_t-2\langle y_i y_{i+\hat{x}}\rangle_t) , \quad (15b)$$

$$\phi_y=k_y+\alpha_y(\bar{u}^2+3\langle y^2\rangle_t-2\langle y_i y_{i+\hat{y}}\rangle_t) , \quad (15c)$$

$$\bar{u}^2=\frac{1}{2C}[B'+(B'^2-4A'C)^{1/2}] \text{ or } \bar{u}=0 , \quad (15d)$$

with the definitions

$$A' \equiv A - 3B\langle y^2\rangle_t + 5C\langle y^4\rangle_t + 2\alpha_x(\langle y^2\rangle_t - \langle y_i y_{i+\hat{x}}\rangle_t) + 2\alpha_y(\langle y^2\rangle_t - \langle y_i y_{i+\hat{y}}\rangle_t) , \tag{15e}$$

$$B' \equiv B - 10C\langle y^2\rangle_t .$$

This is a direct extension of the one-dimensional result.[15] The choice of the value of $\bar{u}^2$ is made by determining that which gives the lowest free energy; SCPT predicts a transition at the temperature T_1 where the free energies become equal.

The self-consistency aspect of the above equations may be made more clear by noting that the harmonic coupling constants depend upon averages of the form

$$\langle y_i y_j\rangle_t = \frac{1}{N}\sum_{\mathbf{q}} \frac{T}{\omega^2(\mathbf{q})}\cos[\mathbf{q}\cdot(\mathbf{j}-\mathbf{i})] ; \tag{16}$$

$\omega^2(\mathbf{q})$ depends upon $\langle y_i y_j\rangle_t$ through Eq. (15). Also note that such correlations should be small for systems in which SCPT will work, viz. for anharmonic systems with small amplitude vibrations about the average position. This is useful in evaluating the importance of various contributions to the second-order correction in Eq. (8). Order-of-magnitude estimates may be made by noting that the largest term in the sum in Eq. (16) is the $\mathbf{q}=0$ term; therefore,

$$\langle y_i y_j\rangle_t \le \frac{T}{\Omega^2} \tag{17}$$

with the equality holding only for $\mathbf{i}=\mathbf{j}$.

Using the above equations, the first-order correction reduces to

$$F_1/N = \frac{A}{2}\bar{u}^2 + \frac{B}{4}(3\langle y^2\rangle_t^2 - \bar{u}^4) + \frac{C}{6}(\bar{u}^6 - 30\langle y^2\rangle_t^3 - 45\bar{u}^2\langle y^2\rangle_t^2) - \alpha_x\langle y^2 - y_i y_{i+\hat{x}}\rangle_t\langle 2y^2 - y_i y_{i+\hat{x}}\rangle_t - \alpha_y\langle y^2 - y_i y_{i+\hat{y}}\rangle_t\langle 2y^2 - y_i y_{i+\hat{y}}\rangle_t . \tag{18}$$

The second-order correction is

$$\begin{aligned} F_2/N = -(1/2T)\{&[A - B\bar{u}^2 + C\bar{u}^4 + 3(\alpha_x+\alpha_y - B + \tfrac{10}{3}C\bar{u}^2)\langle y^2\rangle_t + 15C\langle y^2\rangle_t^2 \\ &- \alpha_x(\langle y^2\rangle_t + 2\langle y_i y_{i+\hat{x}}\rangle_t) - \alpha_y(\langle y^2\rangle_t + 2\langle y_i y_{i+\hat{y}}\rangle_t)]^2\bar{u}^2 S_1 \\ &+ [6(\alpha_x+\alpha_y - B + \tfrac{10}{3}C\bar{u}^2 + 10C\langle y^2\rangle_t)^2 + 2(\alpha_x^2+\alpha_y^2)]\bar{u}^2 S_3 \\ &- 12\bar{u}^2[\alpha_x+\alpha_y - B + \tfrac{10}{3}C\bar{u}^2 + 10C\langle y^2\rangle_t](\alpha_x R_{12}^x + \alpha_y R_{12}^y) \\ &+ 12(\alpha_x+\alpha_y - \tfrac{1}{2}B + 5C\bar{u}^2)(\alpha_x R_{22}^x + \alpha_y R_{22}^y)[6(\alpha_x+\alpha_y - \tfrac{1}{2}B + 10C\bar{u}^2)^2 + 7(\alpha_x^2+\alpha_y^2)]S_4 \\ &- 12[\alpha_x^2 + (2\alpha_x + 2\alpha_y - B + 10C\bar{u}^2)\alpha_x + 10C\alpha_x\langle y^2\rangle_t]R_{13}^x \\ &- 12[\alpha_y^2 + (2\alpha_x + 2\alpha_y - B + 10C\bar{u}^2)\alpha_y + 10C\alpha_y\langle y^2\rangle_t]R_{13}^y + 22\alpha_x^2 P_{121}^x + 22\alpha_y^2 P_{121}^y - 12\alpha_x^2 P_{211}^x \\ &- 12\alpha_y^2 P_{211}^y + 4\alpha_y^2\bar{u}^2 P_{111}^y + 120C^2\bar{u}^2 S_5 + 20C^2 S_6 + \alpha_x^2 P_{202}^x + \alpha_y^2 P_{202}^y + 4\alpha_x^2\bar{u}^2 P_{111}^x \\ &+ 4\alpha_x\alpha_y\bar{u}^2[2Q(0,1;1,1;1,0) + Q(0,0;1,1;1,1)] \\ &+ \alpha_x\alpha_y[-12\bar{Q}(0,1;0,0;0,0;1,1) - 12\bar{Q}(0,0;0,0;1,1;1,0) - 6\bar{Q}(0,1;0,1;0,0;1,0) \\ &\quad - 6\bar{Q}(0,1;0,0;1,0;1,0) + 4\bar{Q}(0,1;0,0;1,1;1,0) + \bar{Q}(0,1;0,1;1,0;1,0) \\ &\quad + \bar{Q}(0,0;0,0;1,1;1,1) + 18\bar{Q}(0,1;0,0;0,0;1,0) + 12\bar{Q}(0,0;0,0;0,0;1,1)]\} . \end{aligned} \tag{19}$$

We have introduced the following notation:

$$S_n = \sum_j \langle y_i y_j\rangle_t^n ,$$

$$R_{mn}^x = \sum_j \langle y_i y_j\rangle_t^m \langle y_i y_{j+\hat{x}}\rangle_t^n ,$$

$$R_{mn}^y = \sum_j \langle y_i y_j\rangle_t^m \langle y_i y_{j+\hat{y}}\rangle_t^n ,$$

$$P_{lmn}^x = \sum_j \langle y_i y_j\rangle_t^l \langle y_i y_{j+\hat{x}}\rangle_t^m \langle y_i y_{j+2\hat{x}}\rangle_t^n ,$$

$$P_{lmn}^y = \sum_j \langle y_i y_j\rangle_t^l \langle y_i y_{j+\hat{y}}\rangle_t^m \langle y_i y_{j+2\hat{y}}\rangle_t^n ,$$

$$Q(i_1,j_1;i_2,j_2;i_3,j_3)=\sum_{\mathbf{j}}\langle y_{\mathbf{i}}y_{\mathbf{j}+i_1\hat{\mathbf{x}}+j_1\hat{\mathbf{y}}}\rangle_t\langle y_{\mathbf{i}}y_{\mathbf{j}+i_2\hat{\mathbf{x}}+j_2\hat{\mathbf{y}}}\rangle_t\langle y_{\mathbf{i}}y_{\mathbf{j}+i_3\hat{\mathbf{x}}+j_3\hat{\mathbf{y}}}\rangle_t ,$$

$$\bar{Q}(i_1,j_1;i_2,j_2;i_3,j_3;i_4,j_4)=\sum_{\mathbf{j}}\langle y_{\mathbf{i}}y_{\mathbf{j}+i_1\hat{\mathbf{x}}+j_1\hat{\mathbf{y}}}\rangle_t\langle y_{\mathbf{i}}y_{\mathbf{j}+i_2\hat{\mathbf{x}}+j_2\hat{\mathbf{y}}}\rangle_t\langle y_{\mathbf{i}}y_{\mathbf{j}+i_3\hat{\mathbf{x}}+j_3\hat{\mathbf{y}}}\rangle_t\langle y_{\mathbf{i}}y_{\mathbf{j}+i_4\hat{\mathbf{x}}+j_4\hat{\mathbf{y}}}\rangle_t .$$

Note that these are evaluated by converting to a sum over reciprocal lattice vectors. For instance, we may write S_n as

$$S_n=\frac{1}{N^n}\sum_{\mathbf{j}}\sum_{\mathbf{q}_1\cdots\mathbf{q}_{2n}}\langle y_{\mathbf{q}_1}y_{\mathbf{q}_2}\rangle_t\exp[i\mathbf{q}_2\cdot\mathbf{j}]\cdots\langle y_{\mathbf{q}_{2n-1}}y_{\mathbf{q}_{2n}}\rangle_t\exp[i\mathbf{q}_{2n}\cdot\mathbf{j}]$$

$$=\frac{T^n}{N^{n-1}}\sum_{\mathbf{q}_1\cdots\mathbf{q}_{n-1}}\frac{1}{\omega^2(\mathbf{q}_1)\cdots\omega^2(\mathbf{q}_{n-1})\omega^2(-\mathbf{q}_1-\cdots-\mathbf{q}_{n-1})}+\mathcal{O}(1/N) . \tag{20}$$

Here we have used the results

$$\langle y_{\mathbf{q}_1}y_{\mathbf{q}_2}\rangle_t=\frac{T}{\omega^2(\mathbf{q}_1)}\delta_{\mathbf{q}_1,-\mathbf{q}_2} ,$$
$$\sum_{\mathbf{j}}\exp[i\mathbf{q}\cdot\mathbf{j}]=N\delta_{\mathbf{q},\mathbf{G}} , \tag{21}$$

where $\mathbf{G}$ is any reciprocal lattice vector. We are interested in the limit $N\to\infty$.

While this expression for the second-order correction is complicated, the evaluation is straightforward once the self-consistent parameters have been evaluated. In practice, using Eq. (17) and the fact that the ratio T/Ω^2 will be small for the temperatures of interest, S_5 and S_6 may be neglected. This is advantageous due to the large amount of time required to perform the reciprocal space sums. Similarly, for the low-temperature phase, the terms involving S_4, P_{121}, P_{202}, P_{211}, R_{22}, R_{13}, and $\bar{Q}$ contribute negligibly. (For the high-temperature phase, with $\bar{u}=0$, these are the dominant contributions.)

Thus, we have a prescription for evaluation of the second-order free energy: first, the first-order result in Eq. (9) is evaluated, and minimized with respect to the variational parameters. For our model, this results in the self-consistent equations given above. Next, the second-order correction given in Eq. (8) is evaluated, using the self-consistent values for the parameters. This gives an extremely accurate approximation to the free energy, as shall be shown in the following section.

III. COMPARISON OF APPROXIMATE AND EXACT RESULTS

To test the technique presented in Sec. II, we first use the transfer integral (TI) technique, which allows for the calculation of the exact free energy for systems of size $L_\perp\times L_\parallel$ in the limit $L_\parallel\to\infty$ for small values of $L_\perp$. We present the relevant results of the formalism; the details have been presented elsewhere.[16] (For a recent review of the technique, see the article by Nightingale.[19]) Note that no transition may occur except in the limit $L_\parallel,L_\perp\to\infty$.

We define a transfer integral kernel connecting adjacent rows that is positive, real and symmetric; therefore the eigenvalues λ_n are real and non-negative. Further, the eigenvalues may be labelled such that

$$\lambda_0>\lambda_1\geq\lambda_2\geq\cdots\geq 0 . \tag{22}$$

By enforcing periodic boundary conditions along the direction of the columns, the partition function may be expressed as

$$Z_c=\sum_{n=0}\lambda_n^{L_\parallel}=\lambda_0^{L_\parallel}\left[1+\sum_{n=1}\left[\frac{\lambda_n}{\lambda_0}\right]^{L_\parallel}\right] . \tag{23}$$

In the limit $L_\parallel\to\infty$ the largest term dominates; the configurational free energy per particle is then

$$f\equiv\lim_{L_\parallel\to\infty}\frac{F}{L_\parallel L_\perp}=\lim_{L_\parallel\to\infty}-\frac{T}{L_\parallel L_\perp}\ln Z_c=-\frac{T}{L_\perp}\ln\lambda_0 . \tag{24}$$

Thus, the problem of calculating the free energy is reduced to finding the largest eigenvalue. Numerically this may be done by discretizing the possible displacements, which results in a matrix eigenvalue problem. This is a good numerical approximation, as long as there are a sufficient number of discretized states. However, the size of the matrix is also determined by $L_\perp$, so the size of the system that we may use is limited. In practice, we may only obtain exact TI results for $L_\perp\leq 3$.

In addition to the free energy, we will be interested in the order parameter probability distribution. The probability of finding a *row* of $L_\perp$ particles in the state $\{u_{i1},\ldots,u_{iL_\perp}\}$ may be expressed in terms of the eigenfunction ψ_0 corresponding to the dominant eigenvalue λ_0. Here, u_{ij} indicates the displacement of the particle located at column i, row j. The probability of finding the row in this state is given by

$$P(u_{i1},\ldots,u_{iL_\perp})=\psi_0^2(u_{i1},\ldots,u_{iL_\perp}) . \tag{25}$$

The probability of finding a single particle within the row with the displacement u_{i1} is given by

$$P(u_{i1}) = \int du_{i2} \ldots du_{iL_\perp} P(u_{i1}, \ldots, u_{iL_\perp}) \ . \tag{26}$$

From this, averages of functions of single particle displacements may be calculated using

$$\langle f(u) \rangle = \int du \, P(u) f(u) \ . \tag{27}$$

We may now demonstrate that heterophase fluctuations occur only within a small, finite-size affected regime; this has been discussed more thoroughly elsewhere,[16] but it is important to understand how increasing the system size causes the behavior to approach that of a harmonic lattice. In Fig. 2 we show a schematic drawing of a typical configuration of the system near the bulk transition temperature. The system is divided into domains of the high- and low-temperature phases; these have the average size

$$A = L_\perp \xi_\parallel$$

where $\xi_\parallel$ is the average domain-wall spacing. The domain walls have a characteristic energy $\Sigma L_\perp$, where Σ is related to the domain-wall energy per unit length.[20,21] The domain-wall spacing is related to a Boltzmann factor for the characteristic energy[15,20]

$$\xi_\parallel = \exp\left[\frac{\Sigma L_\perp}{T}\right]$$

and grows exponentially fast with $L_\perp$. For sufficiently large $L_\perp$, the singular part of the free energy (the part with a cusp at the transition) becomes a universal function:[16]

$$f_{\text{sing}}(T, L_\perp) = -\frac{T}{L_\perp \xi_\parallel} W(t) \ , \tag{28}$$

where the reduced temperature is defined to be

$$t = \frac{T - T_1(L_\perp)}{\Delta T(L_\perp)} \ ,$$
$$\Delta T \sim \frac{T_1(L_\perp)}{\Delta S L_\perp \xi_\parallel} = \frac{T_1(L_\perp)}{\Delta S L_\perp} \exp\left[-\frac{\Sigma L_\perp}{T}\right] \ . \tag{29}$$

Here, ΔS is the bulk change of entropy at the transition temperature. [Note that $T_1(L_\perp)$ is defined to be the position of the peak in the heat capacity in order that $\lim_{L_\perp \to \infty} T_1(L_\perp)$ reduces to the bulk transition temperature.] The function $W(t)$ satisfies

$$W(t) \to |t| \quad \text{as} \quad |t| \to \infty$$

in order that the free energy per particle is an intensive variable in the limit that ΔT vanishes, viz., in the limit $L_\perp \to \infty$. This also produces a cusp in the free energy in this limit. For finite $L_\perp$ the cusp is rounded over the temperature range ΔT; thus the finite-size affected regime decreases *exponentially fast* as a function of $L_\perp$. The anharmonic coupling in our model reduces ΔT by increasing the entropy change and by decreasing the bulk transition temperature T_1. By making these couplings sufficiently large, the system becomes *arbitrarily close* to a true phase transition, even in the one-dimensional limit.[16]

In Fig. 3(a), the exact calculation of $\langle u^2 \rangle$ is shown as a function of temperature, for $L_\perp = 1$, 2, and 3. The parameters chosen for the Hamiltonian are $E_{\text{barrier}}/E_{\text{well}} = 2$,

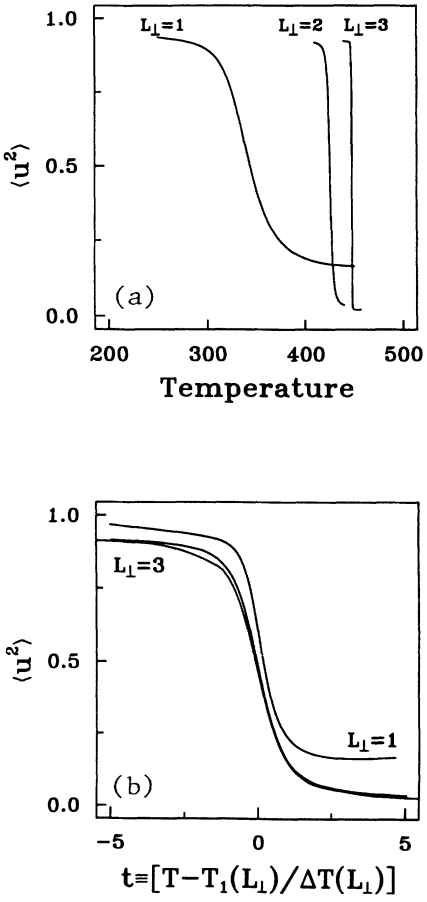

FIG. 3. (a) Average square order parameter $\langle u^2 \rangle$ vs temperature for $L_\perp = 1, 2, 3$. Note the rapid decrease in the rounding as $L_\perp$ gets larger; precursors only occur in this finite-size affected regime. (b) Same data as (a) but graphed as a function of the reduced temperature $[T - T_1(L_\perp)]/\Delta T$. The values of ΔT (see Table I) have been calculated using the transfer-integral technique, according to the scaling result of Eq. (29).

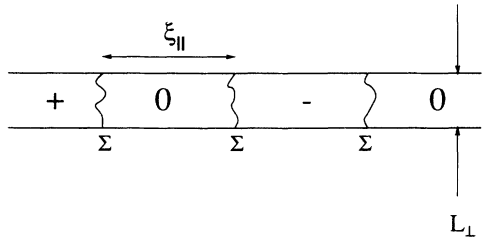

FIG. 2. Schematic of an $L_\perp \times \infty$ system near the bulk transition temperature. The symbols $+, 0, -$ represent regions where the order parameter is positive, zero, and negative, respectively. The domain-wall energy per length is Σ; this energy determines the average domain-wall spacing $\xi_\parallel$.

$k_x = k_y = 8000$, and $\alpha_x = \alpha_y = 4000$. In the limit $L_\perp \to \infty$, the graph would be discontinuous at the transition temperature, corresponding to the discontinuous change in the order parameter, $\langle u \rangle$. For $L_\perp = 1$ the graph of $\langle u^2 \rangle$ shows a broad, finite-size affected regime over which the value of $\langle u^2 \rangle$ changes dramatically. For $L_\perp = 2$ and 3 similar behavior occurs, but over a significantly decreased temperature range. In Fig. 3(b) the same graphs are shown but as a function of the reduced temperature t.

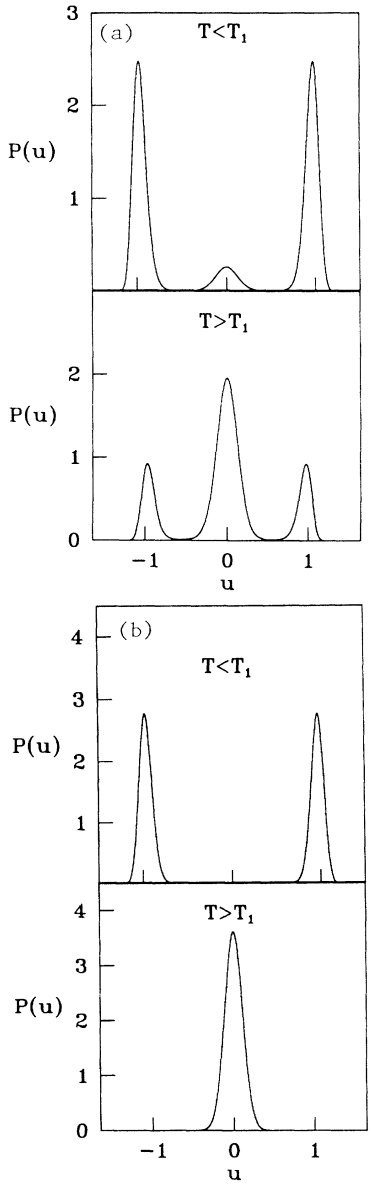

FIG. 4. (a) Probability distribution $P(u)$ for $L_\perp = 1$ at $T = T_1 - 10$ (top graph) and $T = T_1 + 10$ (bottom graph). The small peak in the top graph corresponds to small domains of the high-temperature phase, i.e., heterophase fluctuations. Similarly, the bottom graph shows the presence of heterophase fluctuations into the low-temperature phase. (b) Probability distribution $P(u)$ for $L_\perp = 2$ at $T = T_1 - 10$ (top graph) and $T = T_1 + 10$ (bottom graph). Note the complete absence of heterophase fluctuations.

The approach to a universal function is clear; for larger α this is even more dramatic.[16]

Figure 4(a) shows the probability distribution $P(u)$ for the $L_\perp = 1$ system at $T_1 + \Delta T(L_\perp)/2$ and $T_1 - \Delta T(L_\perp)/2$. Above the transition temperature, the system is predominantly in the center well, i.e., the parent phase. However, a macroscopic portion of the system is in the low-temperature phase (localized in the side wells); this corresponds to heterophase fluctuations—precursors of the low-temperature phase above T_1. Similarly, below T_1, there is a fraction of the system in the high-temperature phase. Figure 4(b) shows the same function for $L_\perp = 2$ at the same temperature offsets; in this case, no evidence of heterophase fluctuations are seen. These are only observable in the finite-size affected temperature range $\Delta T(L_\perp)$, which vanishes rapidly as $L_\perp$ diverges. We expect, therefore, that experimentally observed precursors to the transition are either finite-size effects (for small crystallites), defect-induced transformed regions, or long-lived, non-

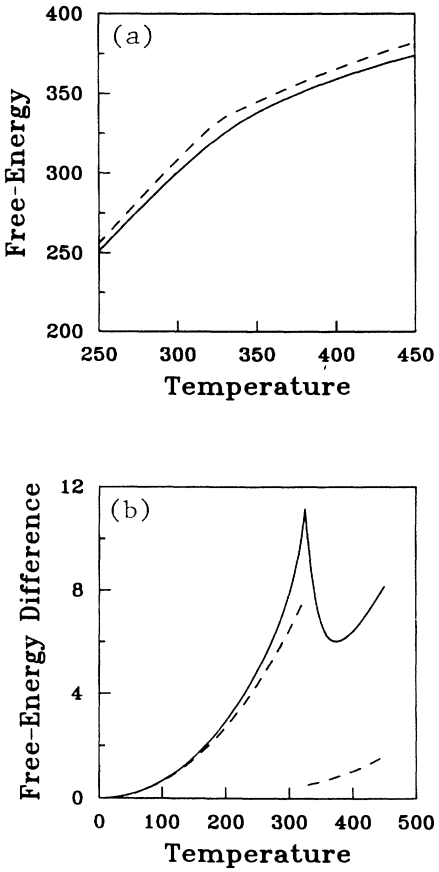

FIG. 5. (a) Exact free energy (solid line) and approximate free energy from first-order SCPT (dashed line) for $L_\perp = 1$. The kink in the SCPT result at $T = 325$ indicates a prediction of a first-order phase transition. (b) The solid line indicates the difference between the exact calculation and the first-order SCPT free energy. The dashed line indicates the magnitude of the second-order correction to the first-order SCPT calculation as a function of temperature. The excellent agreement at low temperatures indicates that the second-order result is considerably more accurate than traditional SCPT.

equilibrium configurations. This is consistent with experiments on pure, high-quality samples.[13] Note that in Fig. 4 the peaks in the probability distribution located near $u=\pm 1$ are not symmetric about the position of the maximum; this indicates that although the system is quite localized, there must be corrections to a purely harmonic description. However, the narrow peaks indicate that the fluctuations are small except within the finite-size affected regime, suggesting that the perturbative approach discussed in Sec. II will be useful.

We may now test our second-order technique by comparing the approximate values with the exact results. In Fig. 5(a) we show the exact free energy, compared with the first-order SCPT prediction calculated using Eq. (18), for $L_\perp=1$. Clearly, the SCPT result is a close approximation to the exact result, especially at low temperatures. Figure 5(b) shows the difference between the two curves, along with the magnitude of the second-order correction calculated using Eq. (19). At low temperatures, the second-order correction accounts for nearly all of the difference, indicating the success of this approach in this temperature range. In the high-temperature phase this does not work as well. For $L_\perp=1$ the system is never completely localized in the center well, and therefore the approximation is not as accurate. Despite this, the approximate free energy is within $\sim 2\%$ of the exact value for all temperatures shown (see Table I).

Figure 6 is similar to Fig. 5, but for $L_\perp=2$. As discussed earlier, and shown in Fig. 4, this system is significantly more localized than the $L_\perp=1$ system. The comparison between the first-order SCPT free energy and the exact value, shown in Fig. 6(a), indicates that SCPT is an excellent approximation. The difference between the curves, shown in Fig. 6(b), is significantly smaller than the $L_\perp=1$ values, especially in the high-temperature phase. Further, the second-order correction accounts for this difference extremely accurately. Table I compares the exact values of the free energy with the first- and second-order SCPT results for $L_\perp=1,2,3$. For $L_\perp=2$ the difference between the second-order SCPT free energy and the exact value is $\lesssim 0.1\%$ of the actual value for all temperatures shown; for $L_\perp=3$ the differences are even smaller. This demonstrates that this second-order approach reproduces the exact results very well in the limit that the system is well localized, viz., in the bulk limit.

We wish to stress that, while both the first- and second-order SCPT calculations improve as $L_\perp$ diverges, we expect the second-order result to have a finite contribution as $L_\perp\to\infty$; this contribution is especially important for calculating the free energy of the low-temperature phase. To demonstrate this, Fig. 7 shows the magnitude of the second-order correction as a function of $1/L_\perp$ at $T=450$, near the bulk transition temperature, for both the low- and high-temperature phases. Both extrapolate to a finite contribution as $1/L_\perp\to 0$. For the high-temperature phase, the limiting value is

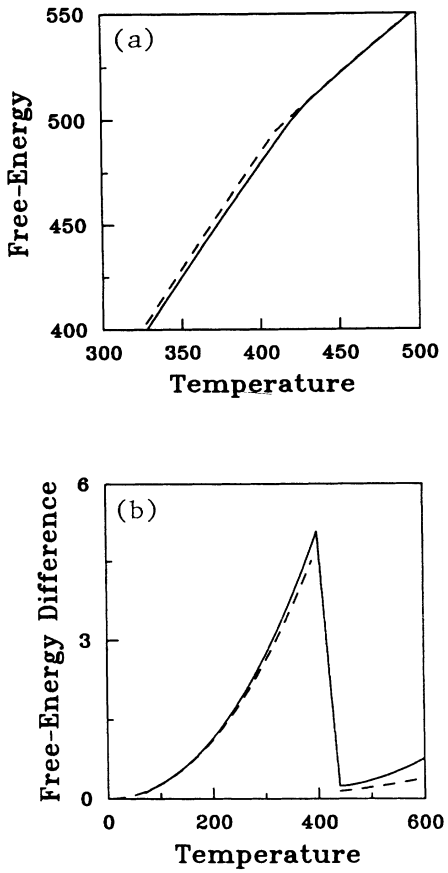

FIG. 6. (a) Exact free energy (solid line) and approximate free energy from first-order SCPT (dashed line) for $L_\perp=2$. The first-order SCPT is more accurate in this case than for $L_\perp=1$ (cf. Fig. 5). (b) As in Fig. 5, we compare the difference between the exact results and the first-order SCPT prediction (solid line) with the correction introduced by using our second-order technique. The comparison is remarkable; the second-order result gives the exact free energy to within 0.1%. The increased agreement (compared to the $L_\perp=1$ case) shows that the behavior of the larger system is increasingly similar to a harmonic crystal.

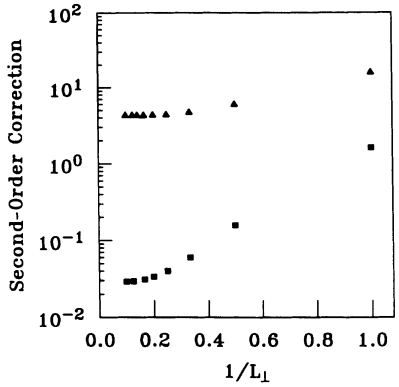

FIG. 7. The magnitude of second-order correction at $T=450$ vs $1/L_\perp$ for low-temperature phase (▲) and high-temperature phase (■). For large systems, the second-order correction to the low-temperature phase is significant, due to the presence of odd-power terms in the expansion of the potential about the absolute minima. The high-temperature phase preserves the $u\to -u$ symmetry; therefore, the second-order correction becomes small in the bulk ($L_\perp\to\infty$) limit.

TABLE I. Comparison of the results for the free energy using the various computational techniques. Note that $\Delta T(L_\perp=1)=40$, $\Delta T(L_\perp=2)=2.76$, and $\Delta T(L_\perp=3)=0.15$. See Table II for $T_1(L_\perp)$.

T	$L_\perp$	F, first-order SCPT	F, second-order SCPT	F, exact
$T_1-2\Delta T$	1	266.86	262.12	261.51
$T_1-\Delta T$	1	308.31	301.85	300.45
T_1	1	340.09	338.19	332.15
$T_1+\Delta T$	1	357.51	356.64	351.46
$T_1+2\Delta T$	1	372.43	371.17	365.41
$T_1-2\Delta T$	2	501.48	499.90	499.45
$T_1-\Delta T$	2	503.36	502.67	502.14
T_1	2	505.22	505.08	504.64
$T_1+\Delta T$	2	507.07	506.95	506.74
$T_1+2\Delta T$	2	508.92	508.80	508.66
$T_1-2\Delta T$	3	537.49	537.43	537.33
$T_1-\Delta T$	3	537.59	537.53	537.48
T_1	3	537.70	537.64	537.62
$T_1+\Delta T$	3	537.80	537.74	537.73
$T_1+2\Delta T$	3	537.91	537.85	537.84

smaller by two orders of magnitude (and significantly less than 0.1% of the total value). Therefore, for large $L_\perp$, we may use the first-order result for the high-temperature phase without losing significant accuracy. This also indicates the importance of using the second-order correction for systems with odd-power anharmonicities: while the first-order SCPT is sufficient for the high-temperature phase, which preserves the $u\rightarrow -u$ symmetry, the second-order technique is required to achieve the same accuracy in the broken-symmetry low-temperature state.

Finally, to give explicit evidence of the necessity of using the second-order SCPT to accurately forecast the thermodynamics of this system, consider Table II. This data shows the transition temperature $T_1(L_\perp)$ as calculated from the first-order SCPT free energy [Eq. (18)], from the second-order SCPT result [Eq. (19)], and from the exact free energy. Clearly the second-order SCPT results are significantly better than the first-order values, in comparison with the exact numbers. There does not seem any reason to believe that the first-order results would ever extrapolate to the bulk limit of the transition temperature. In Fig. 8 the transition temperatures are shown as a function of $1/L_\perp$ (for $L_\perp=64$ we have ignored the second-order contribution to the free energy of the high-temperature phase). The second-order result extrapolates to $T_1=459.7$ in the limit $1/L_\perp\rightarrow 0$; this result should be accurate to $\sim 0.1\%$. Clearly, this is one very useful application of this technique: one is able to extract the bulk transition temperature accurately.

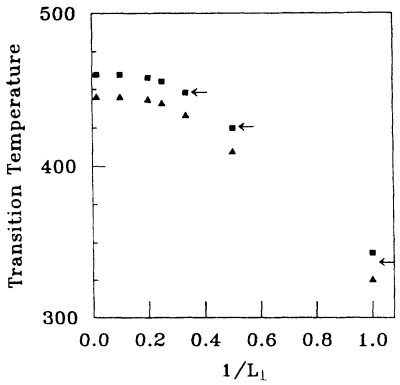

FIG. 8. Predicted transition temperature vs $1/L_\perp$ using first-order SCPT (▲) and second-order SCPT (■). The exact (TI) values for $L_\perp=1,2,3$ are indicated by arrows. The second-order results are considerably more accurate than the first-order results; for $L_\perp=3$ the transition temperature is accurate to 0.1%. We expect the $L_\perp\rightarrow\infty$ extrapolated transition temperature to have a similar (or better) accuracy.

IV. MOLECULAR-DYNAMICS SIMULATIONS

So far our attention has been on the thermodynamic aspects of these systems. As shown in the previous section, in the bulk limit the free energy is very accurately represented by a quasiharmonic theory with perturbative corrections; no precursors, in the sense of being a static equilibrium expectation value are observed in this limit. Prior work[15] has shown that molecular-dynamics (MD) simulations of our model in one-dimension produce

TABLE II. Transition temperature as a function of $L_\perp$ using the various calculational techniques.

$L_\perp$	T_1, first-order SCPT	T_1, second-order SCPT	T_1, exact
1	325.5	343.2	336.9
2	409.8	424.8	425.8
3	433.5	447.9	448.2
4	441.2	455.3	
5	443.6	457.9	
10	445.2	459.6	
64	445.3	459.7	

dynamical structure factors with sharp phonon peaks close to the frequencies predicted by SCPT; we expect that this will be true in the bulk limit as well. However, it remains possible that there may be dynamical correlations due to nonlinear modes that strongly differ from a harmonic description, even in the bulk limit.

In order to extract the dynamic correlations in the bulk limit, we have begun extensive simulations on systems consisting of $L_\perp=1$, 2, and 3 chains of particles for systems with the strip geometry. The advantage of this approach is that we can (and do) verify that the simulations reproduce the exact static quantities, such as $\langle u^2\rangle$, as a check on the possible ergodicity of the simulations. Further, we may examine the dynamical properties at a fixed *reduced* temperature as a function of $L_\perp$; the reduced temperature is given by [cf. Eq. (29)]

$$t\equiv\frac{T-T_1(L_\perp)}{\Delta T(L_\perp)} ,$$

where the values of $T_1(L_\perp)$ and $\Delta T(L_\perp)$ are calculated using the TI technique (see Sec. III as well as Tables I and II). We expect that the dynamical properties, as a function of $L_\perp$ at fixed t, will converge rapidly to the bulk limit, consistent with the convergence of the equilibrium properties. Further, for sufficiently large $L_\perp$, the value of ΔT becomes smaller than the temperature fluctuations in the simulations, so the behavior of the system is indistinguishable from that of a true transition. Here we present a summary of preliminary results of this work; a longer discussion will be presented at a later time.[22]

For conservative MD simulations of first-order transitions near the transition temperature, problems can arise. This is due to the use of the Hamiltonian equations of motion, which conserve energy. The temperature is then defined in terms of the time-averaged kinetic energy of the system:

$$T\equiv 2\frac{\langle E_k\rangle}{N} .$$

Here, N represents the number of configurational degrees of freedom. Near the transition, domains of the low-temperature phase form spontaneously, lowering the average potential energy of the system. As the energy is conserved, the average kinetic energy, and hence the temperature, rises significantly (an example of this problem is given in the work of Kerr *et al.*[23]). This is equivalent to the production of latent heat in a closed system.

In order to avoid these problems, we have used the *constant temperature* equations of motion,[24,25] with an additional degree of freedom γ. The equations of motion for our Hamiltonian H, which we thus consider are given by

$$\begin{aligned}\dot{p}_i&=-\frac{\partial H}{\partial u_i}-\gamma p_i ,\\ \dot{u}_i&=p_i ,\\ \dot{\gamma}&=\frac{1}{M}\left[\sum_i\frac{p_i^2}{T}-N\right] .\end{aligned}\tag{30}$$

These are known as the Nosé-Hoover equations of motion, and are chosen to enforce an average kinetic energy. The value of M governs the rate at which the so-called heat-bath variable γ fluctuates. (Note that we have set the mass of each particle to one, which defines the time scale.)

This formulation for the equations of motion has several advantages: first, the equations of motion are deterministic and reversible. Second, for sufficiently large N, the kinetic energy fluctuations become negligible, so the dynamics approach the original Hamiltonian dynamics. This also occurs in the limit $M\to\infty$. Further, and most importantly, it is straightforward to show[25] that the probability distribution

$$P(\{p_i\},\{u_i\},\gamma)=\frac{1}{Z_0}\exp\left[-\beta H(\{p_i\},\{u_i\})-\frac{M}{2}\gamma^2\right]$$

is stationary under the equations of motion. The variable γ does not affect the probability of the other quantities, so the distribution of $\{p_i\}$, $\{u_i\}$ are those of the canonical ensemble. Integrating the equations of motion and performing averages over a sufficiently long period of time should reproduce the equilibrium canonical values for the given temperature. In practice, the exact (TI) values are reproduced accurately.

We are primarily interested in dynamical correlations, which are potentially sensitive to the altered equations of motion. To test that these correlations are not significantly perturbed, we have calculated the dynamical structure factor, given by

$$D(\mathbf{q},\omega)=\frac{1}{N}\sum_{\mathrm{j}}\int[\langle u_{\mathrm{j}}(t)u_0(0)\rangle-\langle u\rangle^2]e^{i(\mathbf{q}\cdot\mathrm{j}-\omega t)}dt .\tag{31}$$

This is related to the one-phonon contribution to the inelastic neutron-scattering intensity, and provides a sensitive test of the effect of the heat-bath variable on the dynamic correlations. (In practice, we have calculated this repeatedly during each simulation, then averaged over the different spectra.) We have tested that away from the transition temperature and for a sufficiently large value of M, there is no noticeable difference between the spectra calculated using the Hamiltonian equations of motion and those calculated using Eqs. (30). Specifically, phonon peaks were not significantly broadened or shifted by including the heat-bath variable with $M\gtrsim 40$. We conclude that this technique does not alter the dynamics in any important way.

To ensure further that the heat-bath does not affect the dynamics, we have chosen the value of M to be large for temperatures away from the transition, viz., where the temperature fluctuations are small, and to be smaller when the temperature is close to the transition. In particular, we have chosen the form

$$M(T)=M_0\exp\left[\frac{1}{\delta}\left[\frac{T-T_1(L_\perp)}{\Delta T(L_\perp)}\right]^2\right] ,\tag{32}$$

with $M_0=80$ and $\delta=2.485$; the value of δ has been

chosen so that at $T=T_1+2\Delta T$ the "mass" is $M=5M_0$. By choosing this form, the heat-bath variable minimally affects the dynamics of the system away from the transition, when the need for the temperature regulation, or "thermostat," is minimal.

Thus, for each temperature and geometry, we integrate the equation of motions given in Eqs. (30), using the Verlet technique.[26] We have chosen the energy scale so that the barrier height is 300 K k_B, and the length scale to be in Angstroms. By setting the mass scale equal to the mass of the Zr atom, the time scale is approximately equal to 10^{-11} sec. Two thousand Verlet time steps are used per unit time, with averages calculated once every 20 time steps. The system is allowed to equilibrate for $\sim 10^5$ of the averaging time steps, which is equivalent to 10 ns. The averages are calculated over a period of approximately 7 ns. As indicated before, and shown in Ref. 15, the simulations reproduce the exact static quantities very accurately. [Note that the inclusion of the heat-bath variable invalidates the microcanonical expression for the heat capacity,[27] and the fluctuations in the total energy (related to the heat capacity in a canonical system) appear to be sensitive to the heat-bath variable. Therefore we have not been able to accurately calculate the heat capacity. Also, while the average temperature is controlled by this approach, the *fluctuations* in the temperature are still significant.]

In Fig. 9 we present the dynamical structure factor calculated at $T=T_1+3\Delta T$ for $L_\perp=1,2,3$ for $\mathbf{q}=(0.0625,0)$, i.e., one sixteenth of the way to the Brillouin zone. [For the values of $T_1(L_\perp)$ and $\Delta T(L_\perp)$ see Tables I and II.] We have plotted $D(\mathbf{q},\omega)$ on a logarithmic scale to show the features more clearly. In each graph there are three distinct peaks: one near $\omega=0$, a second peak near $\omega=50$, and a small peak near $\omega=125$. The peak near $\omega=50$ is the high-temperature phase phonon peak; note that this is quite sharp for $L_\perp=2$ and 3. For $L_\perp=1$ the central peak near $\omega=0$ is sufficiently large and broad that the phonon peak is not as well defined. The high-frequency peak is associated with low-temperature phase phonons, and is evidence of the long-lived nature of the fluctuations across the barrier. This peak becomes less well defined as the system approaches the bulk limit, consistent with the decreasing time that parts of the system spend in the low-temperature phase.

The most important trend demonstrated in Fig. 9 is that the $\omega=0$ intensity drops rapidly as $L_\perp$ increases. The dominant contribution to this peak appears to be associated with particles crossing over the barrier;[15] thus the intensity of this peak is highest at temperatures close to the transition, i.e., in the finite-size affected regime where precursor fluctuations occur. The rapid decrease of the peak intensity as $L_\perp$ increases indicates that fewer particles are crossing, i.e., the system is more localized within the center well. This is supported by the behavior of the high-temperature phase phonon peak: as $L_\perp$ increases the maximum intensity increases and the width is reduced. In the bulk limit, the contribution to $D(\mathbf{q},\omega)$ arising from long-lived fluctuations into the low-temperature phase will be vanishingly small, and there will be no significant low-temperature phase phonon peak: the dynamical structure factor will exhibit no characteristic behavior indicative of the transition.

In Fig. 10 we present the data at the same temperature

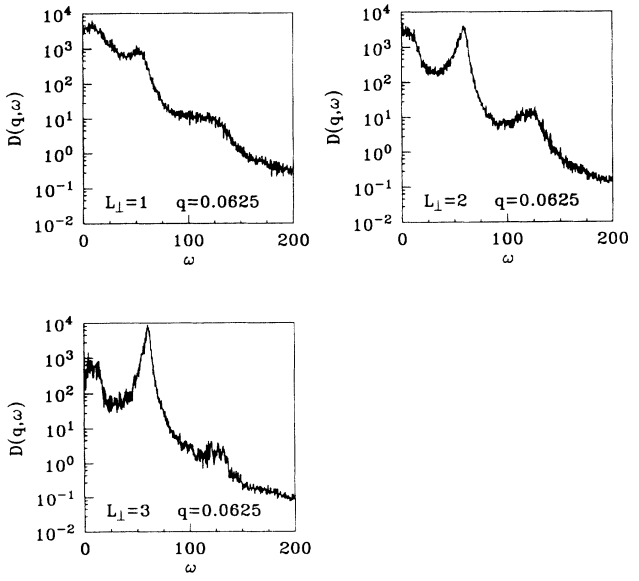

FIG. 9. Dynamical structure factor $D(\mathbf{q},\omega)$ (Fourier transform of the displacement-displacement correlation function) for $\mathbf{q}=(0.0625,0)$ for $L_\perp=1,2,3$. The temperature of each system is $T=T_1(L_\perp)+3\Delta T(L_\perp)$; see Tables I and II for $T_1(L_\perp)$ and $\Delta T(L_\perp)$. Note that the intensity at $\omega=0$ decreases as $L_\perp$ increases; as this occurs, the high-temperature phase phonon peak becomes more intense. The low-temperature phase phonon peak becomes less well defined as $L_\perp$ increases, indicating the decreased occupation of the low-temperature phase.

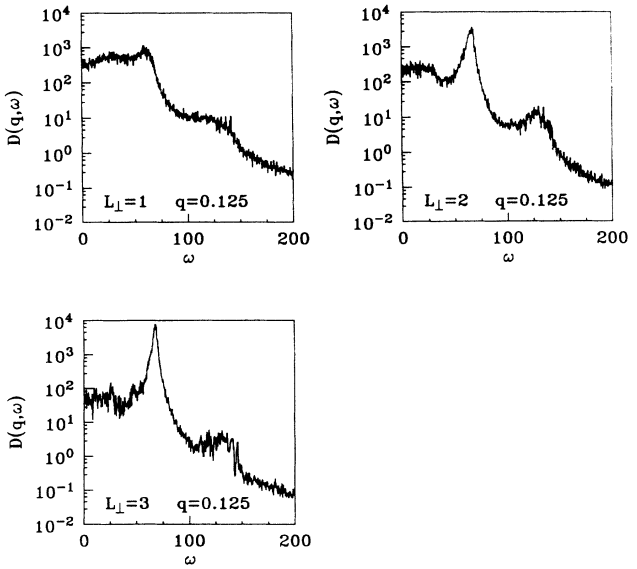

FIG. 10. Dynamical structure factor $D(\mathbf{q},\omega)$ for $\mathbf{q}=(0.125,0)$ for $L_\perp=1,2,3$. The temperatures are the same as in Fig. 9; the intensity at $\omega=0$ decreases as the system size is increased. Phonon peaks become very well defined in the bulk limit.

but at $\mathbf{q}=(0.125,0)$. Comparison with Fig. 9 shows that the intensity at $\omega=0$ drops off rapidly away from $\mathbf{q}=0$. Again, the high-temperature phase phonon peaks become significantly sharper and more intense as $L_\perp$ increases; as this happens, the central peak and the low-temperature phonon peak become poorly defined. Note that for $L_\perp=3$, the central peak intensity is two orders of magnitude less than the phonon peak.

Generally, as the system approaches the transition temperature from above, we see the following features: as a larger fraction of the system occupies the low-temperature phase wells, the central peak grows in intensity, as does the low-temperature phase phonon peak. These both increase as the temperature is lowered; however, at fixed reduced temperature, they decrease as the system size is increased. We expect that the low-temperature phase phonon peak will completely disappear in the bulk limit for $T>T_1$, as the system will then be completely localized.[16] These general features are demonstrated in Figs. 11 and 12, which show the spectra for $L_\perp=1,2$ at $T=T_1+2\Delta T$ and at $T=T_1$, respectively. In these figures, the spectra for $L_\perp=2$ show a sharper, more intense high-temperature phase phonon peak than $L_\perp=1$; concurrently the other features are less pronounced. For $L_\perp=1$ at the transition temperature (Fig. 12), approximately half of the system is in the side well. The low-temperature phase phonon peak is better defined

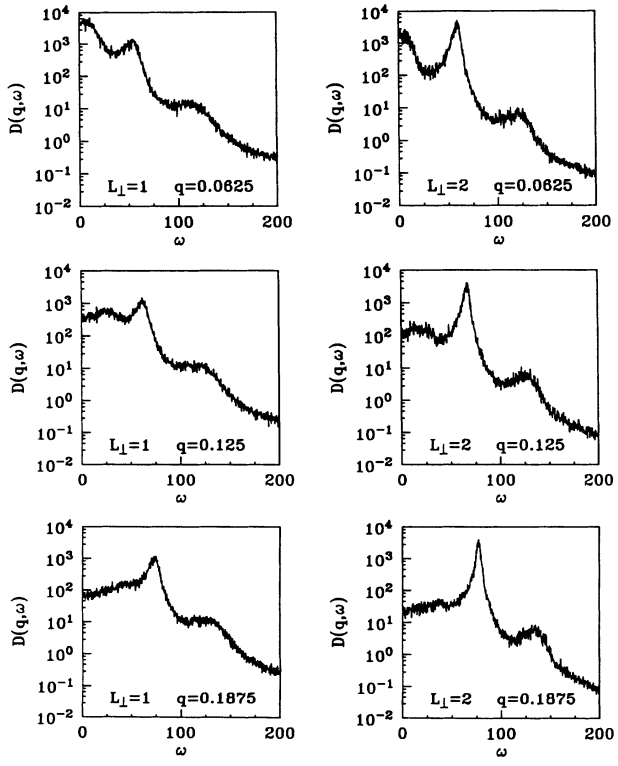

FIG. 11. $D(\mathbf{q},\omega)$ for $\mathbf{q}=(0.0625,0)$, $\mathbf{q}=(0.125,0)$, and $\mathbf{q}=(0.1875,0)$, $L_\perp=1,2$. The temperature is $T=T_1(L_\perp)+2\Delta T(L_\perp)$. The central peak intensity drops off rapidly as a function of q, and the intensity is less for $L_\perp=2$ consistent with Figs. 9 and 10.

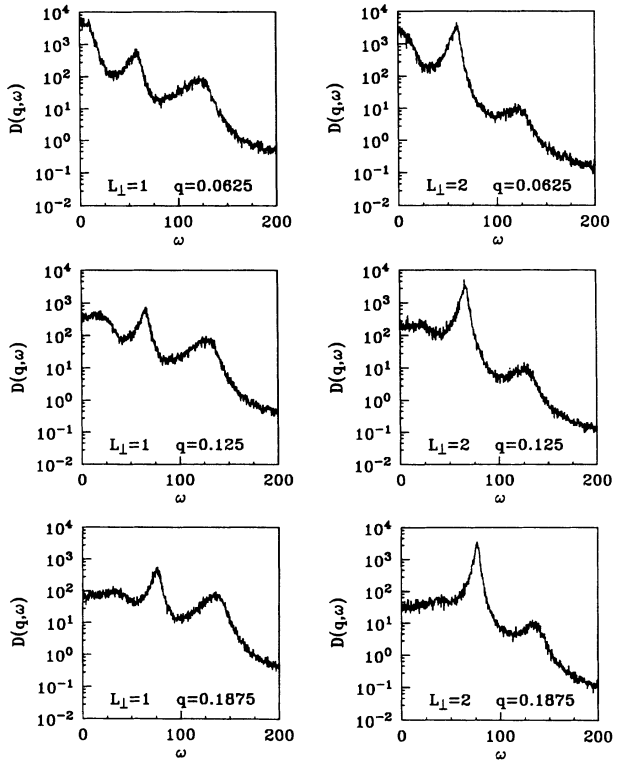

FIG. 12. $D(\mathbf{q},\omega)$ for $\mathbf{q}=(0.0625,0)$, $\mathbf{q}=(0.125,0)$, and $\mathbf{q}=(0.1875,0)$, $L_\perp=1,2$ at the transition temperature. The $L_\perp=1$ system has large domains of the low-temperature phase, thus the low-temperature phase phonon peaks (at higher frequency) have significant intensity. The $L_\perp=2$ system is still predominantly in the high-temperature phase, and the dynamic structure factor is similar to Fig. 11.

and more intense than at higher temperatures. For $L_\perp=2$ there is some hysteresis: the system is still predominantly in the high-temperature phase, and the spectrum is very similar to that shown in Fig. 11.

In the limit that $L_\perp$ is large, the central peak intensity may be small compared to the intensity of the phonon peak; however, there is some evidence that *localized* modes may contribute to a central peak, even in the thermodynamic limit. In Fig. 13 we show the results for the fully transformed systems at $T=T_1-2\Delta T$. At this temperature there is only one phonon peak. The central peak, however, is now well-defined, even at the larger values of q. Furthermore, there is a well defined "cutoff" frequency above which the intensity rapidly drops; this cutoff frequency grows approximately linearly with q. It appears that this peak may indicate an *intrinsic* property of the system, rather than a finite-size effect, as the $L_\perp=1$ and $L_\perp=2$ peaks are of similar intensity.

Very similar features have been seen in simulations on two-dimensional systems with similar Hamiltonians.[23] This feature may be due to localized, large amplitude excitations similar to "breather" modes in the sine-Gordon system.[28] These modes consist of an internal oscillation modulated by an envelope with a significantly lower fre-

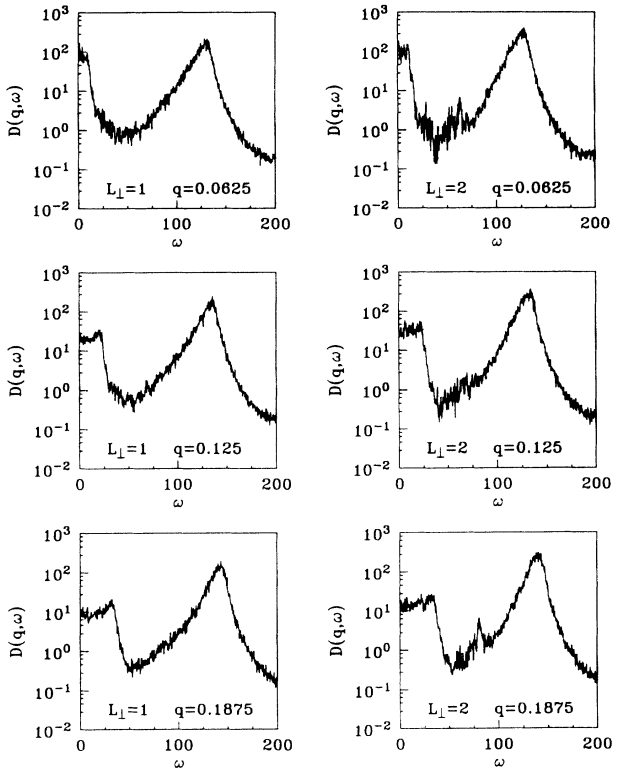

FIG. 13. $D(\mathbf{q},\omega)$ for $\mathbf{q}=(0.0625,0)$, $\mathbf{q}=(0.125,0)$, and $\mathbf{q}=(0.1875,0)$, $L_\perp=1,2$. The temperature is $T=T_1(L_\perp)-2\Delta T(L_\perp)$. Both systems have nearly completely transformed; thus there is no high-temperature phase phonon peak. The central peak is considerably less intense than at higher temperatures, but has a distinctive shape with a very well-defined cutoff frequency.

quency; thus they may contribute to the low-frequency dynamical structure factor. This is in addition to contributions from domain walls, which may explain why these peaks become well defined at low temperatures: at low temperatures, the domain-wall contribution is negligible, and the breather contribution becomes clearer. We have seen breatherlike excitations in real-space trajectories calculated from our simulations; they appear to be reasonably long lived, and are associated with nucleation events. These results, and a more detailed analysis, will be presented later.[22]

V. DISCUSSION

In this paper we have presented an accurate technique for calculating the free energy of a system undergoing a first-order structural phase transition. This technique utilizes self-consistent phonon theory to determine the quasiharmonic phonon frequencies, but goes beyond this approximation by using a second-order expression for the free energy. For a simple model for these transitions, this technique reproduces exact results very accurately, with the error decreasing as the bulk limit is approached. We have extracted a bulk transition temperature that should be accurate to $\lesssim 0.1\%$—this is much more accurate than the first-order self-consistent phonon theory prediction.

As noted in the introduction, SCPT fails when applied to second-order structural transitions.[7] Why, then, does this work so well when applied to first-order transitions? In the former case, when the temperature is slightly above the critical value, the system is characterized by large domains in which the local order parameter, i.e., the displacement, is large; however, the average value over the entire system is zero. The dynamics and thermodynamics are dominated by the critical fluctuations associated with the diverging correlation lengths. For first-order structural transitions, the situation is very different. Above the transition temperature, the system is *entirely* single domain, and the local displacements are small compared with the values characterizing the low-temperature phase. This holds true for all temperatures well below the melting point above the transition. This has been proved rigorously by examining the thermodynamics of a *finite* system and developing a scaling theory to show that there may be coexisting domains only within a narrow finite-size affected regime near the bulk transition temperature.[16] In the thermodynamic limit, coexistence occurs only at the transition temperature. As the local vibrations are relatively small, a quasiharmonic theory based upon expanding the Hamiltonian in powers of the displacement is appropriate. These predictions are further supported by our MD simulations: as the system crosses over from one dimension towards the fully two-dimensional limit, phonon peaks become sharper and more intense, dominating all other nonlinear features.

Recent experiments on Ni_xAl_{1-x} appear to contradict these conclusions. High-resolution electron microscopy experiments on thinned samples show large amplitude distortions toward the low-temperature phase at temperatures well above the transition temperature; elastic neutron-scattering experiments on bulk samples show that these are *static* precursors.[29] However, inelastic neutron-scattering experiments on pure, single crystals of Group IV metals show no such static behavior.[13] Our simulations show dynamic structure factors that are consistent with these latter experiments: the phonon peak positions and widths show weak temperature dependence. In addition, for our system all of the phonon peaks are well defined; the experimentally observed large damping is due to the weak *harmonic* restoring force (allowing large-amplitude vibrations), and has no direct relation to the transition, which depends upon the full, nonlinear potential of the system. We believe that the static local distortions present in Ni_xAl_{1-x} are either due to (i) defects, e.g., concentration fluctuations that dramatically affect the local transition temperature, or (ii) finite-size effects associated with the electro-thinned samples necessitated by the electron microscopy technique.

Now that our approach has been proven effective in calculating the free energy of a simple model, it will be interesting to apply this technique to a real system; however, to do this, it is important to know the anharmonic potential for the ions, preferably from the electron-phonon coupling constants. One system that may be ideal for this type of approach is zirconium; as it is a pure

system, there will be no local concentration effects (an unavoidable defect in alloys), and therefore the predicted behavior may be compared directly to experimental results. Further, the important anharmonicities (but not all) have been calculated from first- principles;[1] using these results, SCPT has been applied to show how the high-temperature bcc phase is stabilized by phonon-phonon couplings.[2] The full prediction of the transition temperature to the hcp phase would be an impressive triumph for this combination of theoretical techniques.

Also of interest is how the dynamics associated with local anharmonicities may be revealed experimentally in bulk systems. Our simulations, as well as results on similar systems,[23] have shown a quasielastic central peak in the dynamic structure factor that has a distinctive shape, i.e., a well-defined cut-off frequency that grows linearly with q. The origin of this feature appears to be due to breather excitations; localized large-amplitude vibrations that distort the system toward the incipient phase. These have been predicted to contribute to the low-frequency response of the system.[28] Similar features have appeared in real-space trajectories in our simulations; these simulations and a detailed analysis of the breather contribution to the central peak will be presented in a forthcoming paper.

ACKNOWLEDGMENTS

We wish to thank Winfried Petry, Steve Shapiro, and Lee Tanner for discussions concerning the experimental work covered in this paper. Also, we wish to thank Alan Bishop, Bruce Harmon, Bill Kerr, Jim Krumhansl, and Vladmir Privman for comments made over the last few years that have helped this theory to reach its present stage of development. We thank Malcolm Stott for a critical reading of this manuscript. We also wish to acknowledge the Advanced Computing Laboratory of Los Alamos National Laboratory, Los Alamos, NM 87545. Many of the simulations were performed on computing resources located at this facility. This work was supported by (U.S.) Department of Energy (DOE) Grant No. DE-FG02-88-ER45364 and by the Natural Science and Engineering Research Council (NSERC) of Canada.

*Current address: Ames Laboratory, Ames, IA 50011-3020.

[1]K.-M. Ho, C.-L. Fu, and B. N. Harmon, Phys. Rev. B **29**, 1575 (1984); Y. Chen, C.-L. Fu, K.-M. Ho, and B. N. Harmon, *ibid.* **31**, 6775 (1985).

[2]Y.-Y. Ye, Y. Chen, K.-M. Ho, B. N. Harmon, and P.-A. Lindgård, Phys. Rev. Lett. **58**, 1769 (1987).

[3]G. L. Zhao and B. N. Harmon, Phys. Rev. B **45**, 2818 (1992).

[4]This ignores the effect of thermal vibrations of the ions on the electronic part of the free energy, which (in principle) should also be included. A discussion of this effect on the total electronic energy is given by P. B. Allen and Volker Heine, J. Phys. C **9**, 2305 (1976).

[5]N. Boccara and G. Sarma, Physics **1**, 219 (1965).

[6]E. Pytte, Phys. Rev. Lett. **28**, 895 (1971).

[7]A. D. Bruce, Adv. Phys. **29**, 111 (1980).

[8]N. R. Werthamer, Phys. Rev. B **1**, 572 (1970); Am. J. Phys. **37**, 763 (1969).

[9]S. Doniach, in *Lattice Dynamics,* edited by R. F. Wallis (Pergamon, New York, 1963), p. 305.

[10]See, e.g., R. A. Cowley, Adv. Phys. **12**, 421 (1964).

[11]R. Peierls, *Quantum Theory of Solids* (Clarendon, Oxford, 1955).

[12]J. A. Krumhansl and R. J. Gooding, Phys. Rev. B **39**, 3047 (1989).

[13]W. Petry, T. Flottmann, A. Heiming, J. Trampenau, M. Alba, and G. Vogl, Phys. Rev. Lett. **61**, 722 (1988); W. Petry *et al.*, Phys. Rev. B **43**, 10933 (1991); **43**, 10948 (1991); **43**, 10963 (1991).

[14]R. J. Gooding, Scr. Metall. **25**, 105 (1991).

[15]J. R. Morris and R. J. Gooding, Phys. Rev. Lett. **65**, 1769 (1990); J. R. Morris and R. J. Gooding, Phys. Rev. B **43**, 6057 (1991).

[16]J. R. Morris and R. J. Gooding, J. Stat. Phys. **67**, 471 (1992).

[17]R. P. Feynman, *Statistical Mechanics* (Benjamin-Cummings, Reading, Massachusetts, 1972).

[18]T. H. K. Barron and M. L. Klein, in *Dynamical Properties of Solids,* edited by G. K. Horton and A. A. Maradudin (North-Holland, Amsterdam, 1974), Vol. 1, p. 391.

[19]M. P. Nightingale, in *Finite-Size Scaling and Numerical Simulation of Statistical Systems,* edited by V. Privman (World Scientific, Singapore, 1990), p. 287.

[20]V. Privman and M. E. Fisher, J. Stat. Phys. **33**, 385 (1983).

[21]E. Brézin and J. Zinn-Justin, Nucl. Phys. B **257 [FS14]**, 867 (1985).

[22]J. R. Morris and R. J. Gooding (unpublished).

[23]W. C. Kerr, A. M. Hawthorne, R. J. Gooding, A. R. Bishop, and J. A. Krumhansl, Phys. Rev. B **45**, 7036 (1992).

[24]S. Nosé, Mol. Phys. **52**, 255 (1984); J. Chem. Phys. **81**, 511 (1984).

[25]W. G. Hoover, Phys. Rev. A **31**, 1695 (1985).

[26]L. Verlet, Phys. Rev. **159**, 98 (1967).

[27]J. L. Lebowitz, J. K. Percus, and L. Verlet, Phys. Rev. **153**, 250 (1967).

[28]A. R. Bishop, J. Phys. A **14**, 1417 (1981).

[29]S. M. Shapiro, B. X. Yang, Y. Noda, L. E. Tanner, and D. Schryvers, Phys. Rev. B **44**, 9301 (1991).